catalysts

MDPI

*Article*

# Production of 14α-Hydroxy Progesterone Using a Steroidal Hydroxylase from *Cochliobolus lunatus* Expressed in *Escherichia coli*

**Yaowen Chang [1], Han Liu [1], Wei Tian [1] and Zunxue Chang [1,2,*]**

[1] School of Life Science and Biopharmaceuticals, Shenyang Pharmaceutical University, Shenyang 110016, China; changyaowen0101@163.com (Y.C.)
[2] Shenyang Botai Biopharmaceutical Co., Ltd., Shenyang 110027, China
* Correspondence: zunxue.chang@syphu.edu.cn

**Abstract:** Steroids with hydroxylation at C14 are drawing increased attention because of their diverse biological activities and applications. *P*-450$_{lun}$ from *Cochliobolus lunatus* is the first fungal cytochrome P450 reported to have 14α-hydroxylase activity. Studies have shown that *P*-450$_{lun}$ catalyzes the hydroxylation of progesterone (PROG) at C14α with low regiospecificity and activity. To improve its regiospecificity and activity for PROG, truncated forms of *P*-450$_{lun}$ and its cognate redox partner CPR$_{lun}$ were functionally co-expressed in *Escherichia coli*. Then, a semi-rational protein engineering approach was applied to *P*-450$_{lun}$, resulting in a double-site mutant E109A/F297W with enhanced 14α-position selectivity for PROG compared with the wild-type *P*-450$_{lun}$ (97% vs. 28%). Protein structure analysis revealed that the F297W substitution can hinder the binding pose for 11β-hydroxylation product formation. Finally, whole-cell catalysis was optimized, and the final titer of 14α-OH-PROG reached 16.0 mg/L. This is the first report where a fungal 14α-hydroxylase was functionally expressed in *Escherichia coli*. The steroid hydroxylation system obtained in this study can serve as a basis for the synthesis of 14α-hydroxylated PROG and the rapid evolution of eukaryotic cytochrome *P*-450$_{lun}$.

**Keywords:** steroid 14α-hydroxylation; 14α-OH progesterone; cytochrome P450; *Cochliobolus lunatus*; *Escherichia coli*



**Citation:** Chang, Y.; Liu, H.; Tian, W.; Chang, Z. Production of 14α-Hydroxy Progesterone Using a Steroidal Hydroxylase from *Cochliobolus lunatus* Expressed in *Escherichia coli*. *Catalysts* **2024**, *14*, 247. https://doi.org/10.3390/catal14040247

Academic Editor: Anwar Sunna

Received: 20 March 2024
Revised: 30 March 2024
Accepted: 4 April 2024
Published: 8 April 2024



## 1. Introduction

Steroids, pervasive terpene lipids in nature, have long served as therapeutic agents for a range of clinical diseases, including rheumatologic, autoimmune, and inflammatory disorders [1,2]. The diverse physiological and pharmacological activities of steroids result from the strategic introduction of various functional groups onto the rigid gonane ring [3,4]. A pivotal modification is the hydroxylation of the steroid backbone, a process that heightens the polarity of hydrophobic steroid molecules, thereby influencing their toxicity, cell membrane penetration ability, and the biological effects of steroid drugs ultimately [5]. Of particular interest are 14-position hydroxylated steroids. 14α-OH steroids exhibit specific biological activities, demonstrating potential antigonadotrophic and anticancer properties [6–8]. In contrast, 14β-OH substituent is normally found in cardiotonic steroids, which are commonly used in treating congestive heart failure because of their cardiac effects, particularly the positive transducer effect [9–11].

Two approaches are currently used to incorporate 14-OH groups into steroids: chemical synthesis and biocatalysis. Nevertheless, the chemical synthesis route for steroid hydroxylation is beset by its complexity, low yields, and environmental unfriendliness [12,13]. In contrast, biocatalysis is gaining prominence because of its high selectivity and atom utilization efficiency [14]. Diverse microorganisms, including prokaryotes and fungi, can efficiently catalyze the production of steroids containing 14α-OH [15,16]. Conversely, only

certain plants and amphibians can yield 14β-hydroxylated sterols in small quantities [17]. Fortunately, 14β-OH steroids can be obtained using the facile conversion of 14α-OH counterparts through chemical methods, enhancing the significance of investigating the biocatalytic synthesis of 14α-OH steroids.

Although many species can produce steroids with 14α-OH, research on the identification and characterization of these hydroxylation genes has been few reported. To our knowledge, 14α-hydroxylases have been obtained from *Cochliobolus lunatus* (anamorph *Curvularia lunatus*) [15,18,19], *Bipolaris* sp. [20], *Thamnidum elegans* [21], *Crocus sativus*, and *Bufo toadstool* [17]. In contrast, the 14β-hydroxylases remain elusive. Although *Crocus sativus* and *Bufo toadstool* can produce 14β-hydroxylated steroids, the results of transcriptome data analysis and P450 gene screening experiments only proved the existence of 14α hydroxylation genes [17]. This fact supports the hypothesis that nature exhibits a preference for generating 14α-OH, subsequently undergoing conformational conversion to 14β-OH through processes such as dehydration and hydration.

Two 14α-hydroxylases have been obtained from *Cochliobolus lunatus*: *P*-450$_{lun}$ (from *C. lunatus* ATCCTM12017, equivalent to CYP103168 from *C. lunatus* CECT 2130) [15,19] and CYP14A (from *C. lunatus* CGMCC 3.3589 and *C. lunatus* JTU 2.406) [18]. The corresponding electron transport protein, CPR$_{lun}$, was identified using transcriptome analysis and genetic screening. *P*-450$_{lun}$ and CYP14A, with approximately 82% sequence identity, all have low C14-hydroxylation specificity for C17-substituted steroids, such as progesterone (PROG), when co-expressed with CPR$_{lun}$ in *Saccharomyces cerevisiae* [15,18]. Specifically, *P*-450$_{lun}$ converts PROG into a mixture of products with 14α-OH and 11β-OH at a 1:1 ratio [18]. PROG is the fundamental steroidal core for synthesizing C21 steroid derivatives of pharmaceutical significance. 14-OH-PROG is a crucial intermediate in the chemical and biological synthesis of active steroids, such as cardenolides [10,22]. Therefore, we performed engineering of *P*-450$_{lun}$ to enhance its C14 regioselective hydroxylation of PROG in this study.

Yeasts are the primary choice for the heterologous expression of membrane-bound eukaryotic cytochrome P450 (CYP) because the composition and structure of the endoplasmic reticulum membrane of yeast cells allow the anchoring of membrane-bound proteins [23,24]. The reported 14α-hydroxylases such as CYP11411, CYP44476, *P*-450$_{lun}$ and CYP14A all employed *S. cerevisiae* as the host for investigating the transformation of steroid substrates [17]. However, this expression system also comes with some drawbacks, including the unexpected formation of by-products, altered protein glycosylation, challenges in predicting plasma membrane permeability for specific compounds, and unpredictable targeting of recombinant proteins [25]. Moreover, the burdensome operation and slow growth rate of yeasts limit the size and screening speed of mutant libraries for the directed evolution of enzymes with low activity and selectivity [23,26]. Here, we propose using *E. coli* as an expression system because of its successful use in the heterologous expression of mammalian or fungal CYPs and operational convenience during enzyme directed evolution.

In this study, we report the functionally heterologous co-expression of N-terminally modified *P*-450$_{lun}$ and CPR$_{lun}$ in *E. coli*. We also engineered the truncated *P*-450$_{lun}$, resulting in a double-site mutant (E81A/F269W) with enhanced regioselectivity and activity for the C14α hydroxylation of PROG. Finally, the whole-cell catalysis was optimized, and the production of 14α-OH-PROG was further increased. This is the first report of producing 14α-OH-PROG in *E. coli* with a fungal 14α-hydroxylase.

## 2. Results and Discussion

### *2.1. Identification of a Functional Truncated Form of P-450$_{lun}$ (ΔP-450$_{lun}$)*

The *P-450$_{lun}$* and *CPR$_{lun}$* were chemically synthesized and codon-optimized for expression in *E. coli*. As a redox partner, Flavin adenine dinucleotide (FAD) and flavin mononucleotide (FMN) containing CPR$_{lun}$ mediates electron transfer and is essential for *P*-450$_{lun}$ catalytic activity [14,27,28]. Class II P450 *P*-450$_{lun}$ and its partners CPR$_{lun}$ can be typically co-expressed in a vector system using one or two "promoter-ORF(s)-terminator" expression cassettes [29]. With the single cassette approach, *P*-450$_{lun}$ and CPR$_{lun}$ can be

spaced apart by a sequence containing the ribosome entry/binding site, and two distinct proteins will be expressed. The expression of the *P*-450$_{lun}$ and CPR$_{lun}$ will be heterogeneous, with the upstream gene displaying higher expression [30,31]. In addition, *P*-450$_{lun}$ and CPR$_{lun}$ can also be linked by a nucleotide sequence (can be translated into a flexible or rigid linker) and expressed as a fusion protein. However, the nucleotide length and amino acid composition can severely affect the activity of the fusion protein [32–34]. To avoid variability in expression efficiency and the selection of complex linkers, plasmid pRSFDuet with two expression cassettes was applied to express *P*-450$_{lun}$ and CPR$_{lun}$.

As membrane-bound proteins, eukaryotic *P*-450$_{lun}$ and its cognate partner CPR$_{lun}$ possess N-terminal hydrophobic domains (residues 2–29 and 2–31, respectively) that anchor to the plasma membrane. However, *E. coli* lacks membrane-bound organelles, potentially leading to inclusion body formation or low protein expression due to its poor recognition ability of unique signaling sequences when expressing membrane-bound proteins [26,35]. Fortunately, these limitations can be addressed by N-terminal modifications, including amino acid substitutions and truncations of hydrophilic sequences [26,36,37].

Firstly, we produced a recombinant *E. coli* BL21 (DE3) strain containing a modified *P-450$_{lun}$* (by replacing the second codon with alanine or substituting the N-terminal region with the hydrophilic sequences MAKKTSS or MALLLAVFL) [38–40] and Δ*CPR$_{lun}$* (containing a truncated transmembrane region), while no detectable by-products of PROG were produced during whole-cell biotransformation. Then, transmembrane helices truncated *P*-450$_{lun}$ and CPR$_{lun}$ (Δ*P*-450$_{lun}$ and Δ*CPR$_{lun}$*, respectively) were introduced into *E. coli* BL21 (DE3), and detected products were generated (Figure 1A). High-performance liquid chromatography (HPLC) analyses revealed that PROG was converted into two major compounds and several uncharacterized hydroxylated by-products. Isolation, purification, and structural analysis using nuclear magnetic resonance (NMR) of the main compounds showed that they were 14α-OH-PROG and 11β-OH-PROG, respectively (with ratio of ~2:1) (Figure 1B; see NMR Data and spectrums in the Supporting Information). While the molar ratio of 14α-OH-PROG/11β-OH-PROG was different from that obtained from 1:1 in *S. Cerevisiae*, this could be the result of different culture conditions such as the pH, incubation time, and substrate dose [18]. Therefore, the N-terminally modified *P*-450$_{lun}$ and CPR$_{lun}$ from *C. lunatus* were functionally expressed in *E. coli*. However, the activity and regioselectivity of Δ*P*-450$_{lun}$ for C14α position were still low (approximately 21% yield at a concentration of 3.5 mg/L).

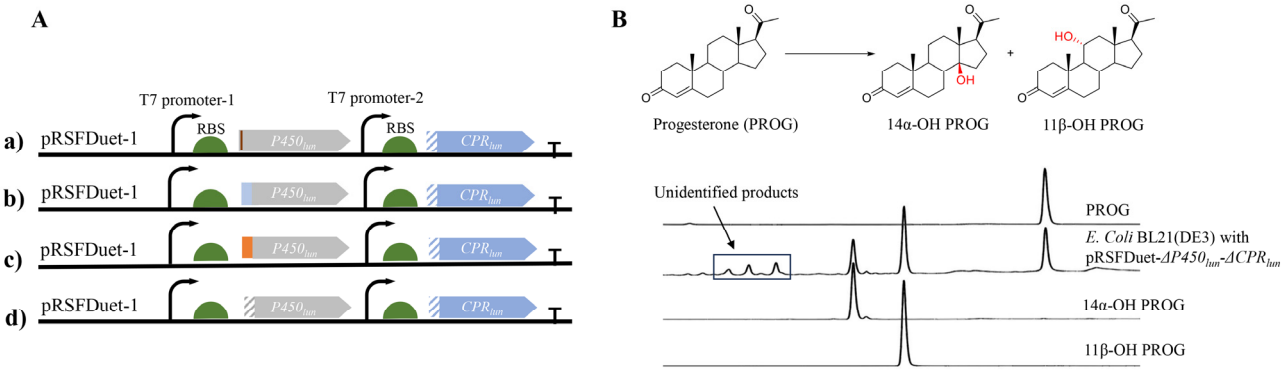


**Figure 1.** (**A**) The configuration of plasmids pRSFDuet containing modified *P*-450$_{lun}$ with its cognate partner ΔCPR$_{lun}$ (with amino acids 2–31 truncated). (**a**) Substitute the second amino acid Asp of *P*-450$_{lun}$ with Ala. (**b**) Amino acids 2–29 of *P*-450lun were truncated. (**c**) Substituting the transmembrane region (amino acids 2–29) of *P*-450$_{lun}$ with AKKTSS. (**d**) Substituting the transmembrane region of *P*-450$_{lun}$ with ALLLAVFL. (**B**) The HPLC profiles of PROG biotransformation with recombinant *E. coli* containing pRSFDuet_Δ*P*-450$_{lun}$_ΔCPR$_{lun}$. Reaction conditions: 50 g cww/L recombinant *E. coli* cells were suspended in phosphate buffer (pH 7.4, 50 mM) containing 50 μM PROG; reactions were conducted at 28 °C, 250 rpm for 8 h.

### 2.2. Engineering Δ*P*-450$_{lun}$ to Improve Its Regiospecificity and Catalytic Activity

In pursuit of refining the regiospecificity of Δ*P*-450$_{\text{lun}}$ at C-14α of PROG, a hybrid approach involving a semi-rational design and directed evolution was employed. Given that the crystal structure of *P*-450$_{\text{lun}}$ is not available, a three-dimensional model was constructed using SWISS-MODEL [41] based on the crystal structure of CYP3A4 (PDB ID 5VCD, identity: 28%; similarity: 46%) [42]. Although the sequence identity is not high, they possess a comparable overall fold and a conserved heme-binding core structure [43]. To enhance model accuracy, GalaxyRefine [44,45] and Gromacs [46] were employed for side-chain repacking and global structural relaxation, resulting in an optimized model with an initial *Z*-score [47] of −8.25 (Figure S1) and more than 91.0% of residues located in the most favored regions of the Ramachandran plot [48,49] (Figure S2).

Molecular docking of PROG into the presumed structure of Δ*P*-450$_{\text{lun}}$ was conducted to identify residues potentially influencing selectivity. The analysis of docking poses with the lowest binding free energy revealed two distinct binding modes (pose I and II), corresponding to 14α- and 11β-hydroxylation, respectively (Figure 2A). The lower free energy associated with mode II suggests a preference for 11β-OH. In this mode, the four-ring structure of PROG assumed a slightly oblique orientation to the heme ring, and its β-side faced the heme group. The C17 acetyl group of PROG was close to the I-helix and formed hydrogen bonds with His121 and Ser294. While in pose I, the ligand rotated its plane by approximately 180°, so the α-side faced the heme group. This binding mode was stabilized by a hydrogen bond between the C20-keto group of PROG and Thr369 and the hydrophobic interaction of the gonane ring structure with residues Phe297, Ala298, and Met365 (Figure 2B).

Molecular docking also showed the presence of eight residues (P108, E109, L122, S294. F297, T364, S367, and F368) within 5 Å of the ligands in both binding modes (Figure 2C). P108, E109, and L122 were located in substrate recognition site 1 (SRS-1). Residues S294 and F297 were located in the I-helix near the conserved sequence motif AGXXT (325–329), which was involved in selectivity. Residues T364, S367, and F368 were located at positions +5, +8, and +9 in the highly conserved EXXR motif in SRS-5. Given their proximity to the heme group, these three residues had a high potential for substrate binding and control of regioselectivity [50]. We hypothesized that these eight residues contributed to the selectivity or activity of Δ*P*-450$_{\text{lun}}$ and that replacing these amino acids could improve the activity or selectivity of hydroxylation at C14α.

Alanine scanning was performed across the eight residues to identify the key residues with a remarkable substantial effect on region-selectivity or activity. The substitutions E109A and F297A significantly improved the selectivity from 28% in the wild type to 57% and 73%, respectively. E109A also increased the PROG conversion from 75% to 83%. Although F297A decreased the conversion to 8%, only a trace amount of by-products was detected (Figure 2D). Motivated by these findings, E109 and F297 were selected for further analyses. We performed site saturation mutagenesis in these two residues using NNK codons in 24-well plates. To achieve a 95% coverage of all possible library variants, approximately 60 variants were screened in each single-site library. HPLC results showed that all screened E109 substitutions displayed similar or decreased PROG conversion and selectivity compared to E109A. Conversely, F297W substitution had the highest PROG conversion (41%) and selectivity (93%). To further enhance the regioselectivity and activity of Δ*P*-450$_{\text{lun}}$, we combined these two substitutions to obtain a double mutant E109A/F297W, which had higher selectivity (approximately 97%) and catalytic activity (Figure 3A,B; Table 1).

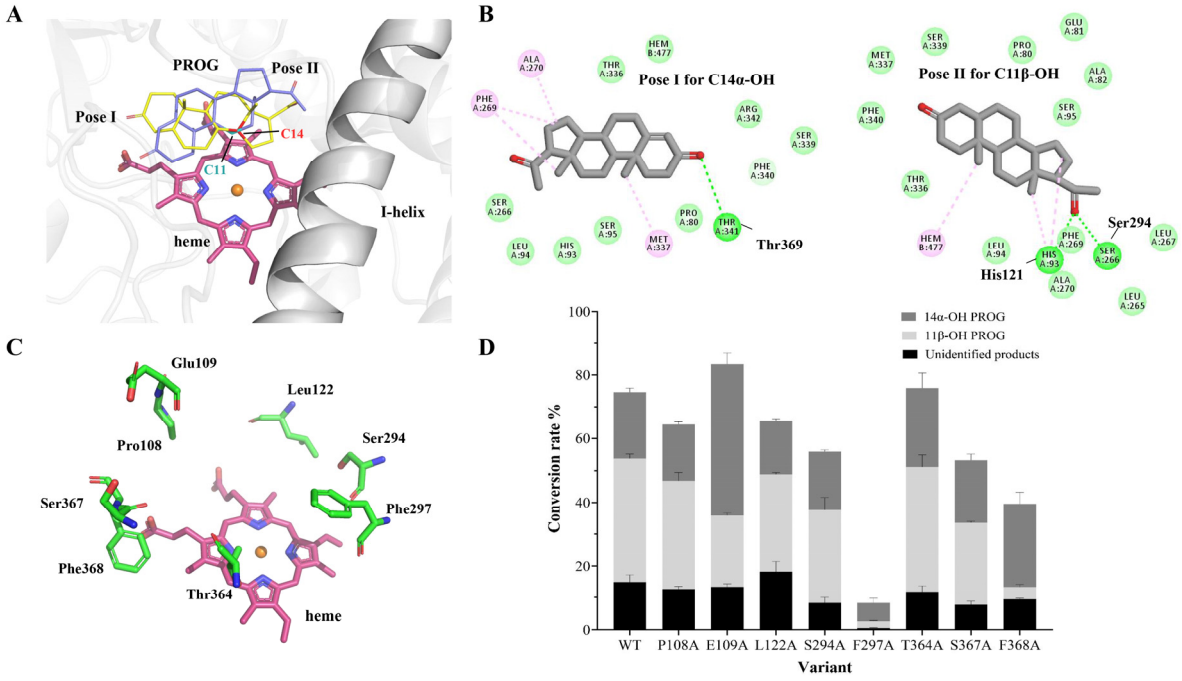


**Figure 2.** (**A**) Superposition of the results from docking PROG in the homology model of Δ*P*-450$_{lun}$. Yellow: docking pose I for the hydroxylation at C14α of PROG; purple: Docking pose II for the hydroxylation at C11β of PROG. (**B**) Interactions between PROG and Δ*P*-450$_{lun}$ in pose I and pose II. Analyzed using Discovery Studio Visualizer. Green dash: conventional hydrogen. Pink dash: hydrophobic (Pi-Alkyl). Residue numbering in bold corresponds to the long form of *P*-450$_{lun}$ and the circles to Δ*P*-450$_{lun}$. (**C**) Superposition of selected amino acids for Alanine-scanning mutagenesis. (**D**) Whole-cell biocatalysis results of different Alanine substitution mutants in *E. coli*. Reaction conditions: 50 g cww/L recombinant *E. coli* cells were suspended in phosphate buffer (pH 7.4, 50 mM) containing 50 μM PROG; reactions were conducted at 28 °C, 250 rpm for 8 h. Error bars are standard deviation for three independent experiments.

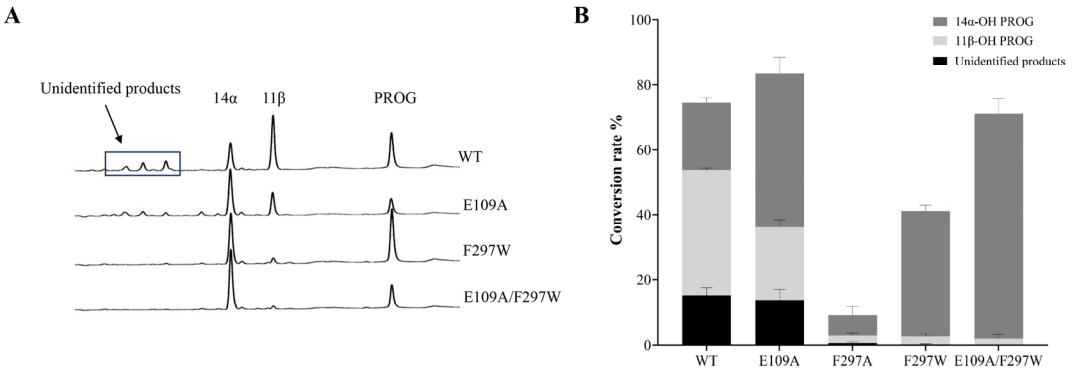


**Figure 3.** Bioconversion of PROG using WT *P*-450$_{lun}$ and its mutants. (**A**) HPLC assay of PROG biotransformation using *E. coli* cells containing pRSFDuet-Δ*P*-450$_{lun}$-ΔCPR$_{lun}$ and positive mutants of Δ*P*-450$_{lun}$. (**B**) Distribution of the products of PROG using WT and corresponding mutants (E109A, F297A, F297W and E109A/F297W). Reaction conditions: 50 g cww/L recombinant *E. coli* cells were suspended in phosphate buffer (pH 7.4, 50 mM) containing 50 μM PROG; reactions were conducted at 28 °C, 250 rpm for 12 h. Error bars are standard deviation for three independent experiments.

**Table 1.** Conversion rate of PROG hydroxylation and product distribution of *P*-450$_{lun}$ and mutants from the bioconversion assay.

| Mutants | Conversion (%) [1] | Selectivity (%) | | |
|---|---|---|---|---|
| | | 14α | 11β | Others |
| WT | 75 | 28 | 52 | 20 |
| E109A | 84 | 57 | 27 | 16 |
| F297A | 9 | 69 | 26 | 6 |
| F297W | 41 | 93 | 6 | 1 |
| E109A/F297W | 71 | 97 | 2 | 1 |

[1] Reaction conditions: recombinant *E. coli* cells were suspended in phosphate buffer (pH 7.4, 50 mM) containing 50 μM PROG; reactions were conducted at 28 °C, 250 rpm for 8 h.

### 2.3. Computational Analysis of Δ*P*-450$_{lun}$ and Its Variants

Structural and computational analyses were performed to understand the molecular basis for the selectivity and activity difference between Δ*P*-450$_{lun}$ and its mutants for PROG. The binding modes of PROG in Δ*P*-450$_{lun}$ were identical to PROG-bound CYP260A1, which can catalyze hydroxylation of PROG at C1α or C17α [51]. Molecular docking revealed that the introduction of the larger indole group in F297W reduced the binding pocket volume of Δ*P*-450$_{lun}$ by 168.5 Å$^3$ and brought in a significant steric hindrance against the substrate in pose I (Figure S7 and Figure 4C). The shift in selectivity might arise from the destabilization of the alternative binding mode due to the steric hindrance and hydrogen bond disruption caused by F297W.

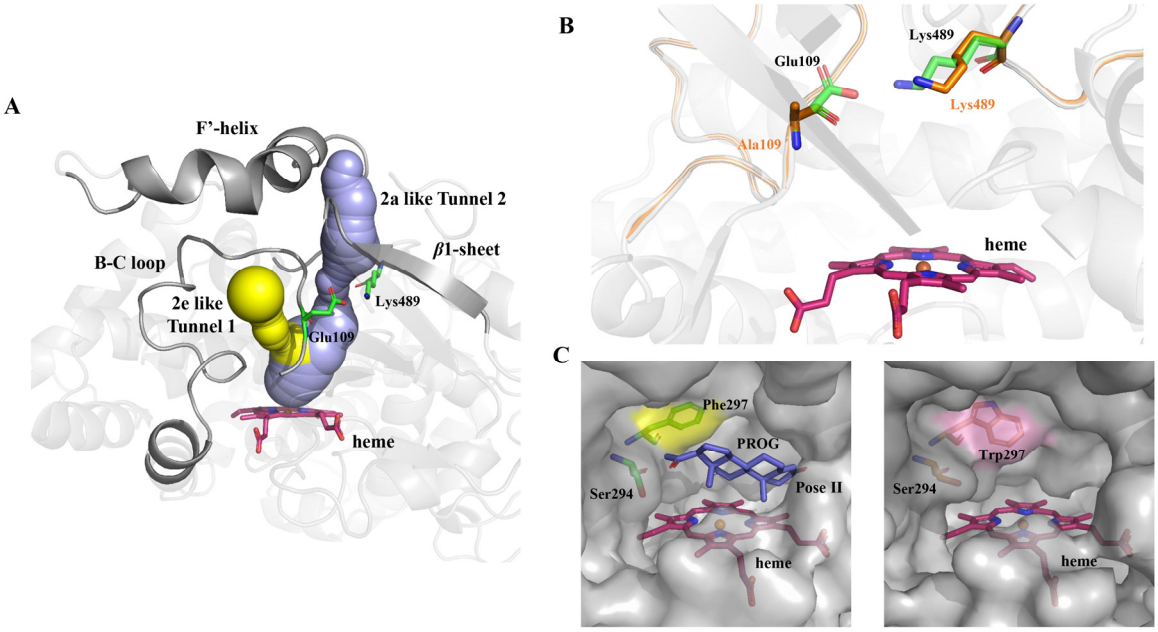


**Figure 4.** Channels and structural analyses of Δ*P*-450$_{lun}$ and its positive variants. (**A**) The trajectories of 2a-like channel and 2e-like channel in Δ*P*-450$_{lun}$. The surface models of 2a-like channel and 2e-like channel are colored in purple and yellow, respectively. The adjacent secondary structures are colored in grey. The important residues Glu109 and Lys489 near the node are colored in green, and heme is colored in rose. (**B**) Superposition of the residues 109 and Lys489 in the model of Δ*P*-450$_{lun}$ (grey) and E109A variant (orange). The E109A substitution broke the ionic bond between Glu109 and Lys489, resulting in the increase in distance between residues 109 and Lys489. (**C**) Structural comparison of Δ*P*-450$_{lun}$ and mutants F297W. Surface of Phe297 (green) and Trp297 (orange) are shown as yellow and pink, respectively. In the WT structure, PROG could be docked in the Pose II, resulting in hydroxylation at C11β. F269W substitution might hinder the formation of this binding pose.

Access tunnels facilitate the movement of ligands between the active site and solvent environment, particularly in enzymes with a buried active site [52,53]. Using the Caver3.0 server [54], we identified two distinctive access tunnels in Δ*P*-450$_{lun}$ with features shared by cytochrome P450s [55] (Figure 4A). Tunnel 1, located between the F' helix, B–C loop, and β1 sheet, behaved as a 2a-like channel. In contrast, Tunnel 2, regressed through the B–C loop, could be merged and behaved as a 2e-like channel. Both channels were located in the P450 region involved in substrate specificity.

Detailed analysis revealed that the trajectories of these two channels converged at a node near the heme moiety. Residue E109, situated at the intersection of these two channels, might act as a gate controlling the spatial size of the node. E109 also could form an ionic bond with K489, serving as a critical bottleneck in access Tunnel 1. Therefore, substituting E109 with alanine widened both channels (bottleneck radius increased from 1.36 Å to 1.94 Å for Tunnel 1, from 1.23 Å to 1.50 Å for Tunnel 2) (Figure 4A,B). This modification might enhance the channel's suitability for substrate and water transport, consequently elevating the overall activity of Δ*P*-450$_{lun}$. Moreover, changes in the size, physicochemical properties, or dynamics of the access tunnels of an enzyme can affect its regioselectivity and catalytic activity. Cheng et al. found that a single residue mutation in the access tunnel of *Pp*NHase or *Ct*NHase could invert its regioselectivity toward aliphatic α,ω-dinitriles [56]. Meng et al. replaced the bottleneck residue F79 in the access tunnel of P450$_{Bs\beta}$HI with relatively small amino acid alanine resulting the change of hydroxylation products' distribution toward myristic acid and pentadecanoic acid [57]. So, substituting residue E109, which was located at the end of the access tunnel and the entrance to the binding pocket, with Alanine might contribute to the difference in the size and shape of the substrate access tunnel, and thus resulted in the diversity of reaction regioselectivity [56].

### *2.4. Optimizing the Conditions of Whole-Cell Biocatalyst*

To establish the optimal conditions for whole-cell biocatalysis, various parameters of the biotransformation process, including temperature, pH, and the additives, were systematically evaluated. A preliminary analysis showed the highest yield of 14α-OH-PROG obtained by Δ*P*-450$_{lun}$E109A/F297W. Therefore, we used the *E. coli* strain containing pRSFDuet_Δ*P*-450$_{lun}$E109A/F297W_ΔCPR$_{lun}$ to analyze the effects of different reaction conditions on 14α-OH-PROG yield. Results showed that the optimal reaction temperature and pH were 30 °C and 7.4 (50 mM phosphate buffer), respectively (Figure 5A,B). Subsequent reaction variables were all evaluated under these conditions.

Since P450s are heme-containing enzymes, enhancing the intracellular concentrations of heme can potentially enhance the activity of whole-cell biocatalysts. We investigated the impact of adding different heme precursors, such as hemin, 5-ALA, and $FeSO_4 \cdot 7H_2O$ during the expression of *P*-450$_{lun}$ [58]. Given the limited import of heme into the BL21 (DE3) strain [59], adding heme did not significantly increase 14α-OH-PROG yield. However, supplementation with 5-ALA demonstrated an improvement, achieving the highest yield of 12.7 mg/L when 0.5 mM ALA was added (Figure 5C). In contrast, only trace amount of products were observed in the absence of 5-ALA during the induction of *P*-450$_{lun}$, indicating that *E. coli* relied mainly on exogenous 5-ALA for the biosynthesis of heme. Furthermore, the inclusion of iron might also contribute to the biosynthesis of heme. Adding 0.5 mM ALA to the medium and varying final concentrations of $FeSO_4 \cdot 7H_2O$ (5, 10, 20, 30, and 40 mg/L) were introduced, while no noticeable change in 14α-OH-PROG yield was observed.

As a member of class II P450s, *P*-450$_{lun}$ requires two electrons from NADPH delivered by CPR$_{lun}$ to increase its catalytic activity [14,27]. Thus, the nicotinamide cofactor may also be a limitation in current whole-cell systems. Various concentrations of NADPH (1, 1.5, or 2 equivalents) were introduced to the biotransformation system, and the production of 14α-OH-PROG was assessed at different time points (Figure 5D). The results were compared with the control reaction (without supplemented NADPH). The findings revealed that additional NADPH increased the initial rates and conversions, suggesting that the

regeneration of the cofactor in cells was insufficient to sustain the catalytic reaction at the achieved rates and with the current coupling efficiency. Growth was interrupted when 1.5 equivalents of NADPH were added to the reaction system, possibly due to the low protein expression levels of *P*-450$_{lun}$ or CPR$_{lun}$. These results indicated that introducing the enzymatic regeneration systems (such as GDH/glucose) in the host as a substitute for nicotinamide cofactors may represent an economical approach to produce 14α-OH-PROG in this system. Following the analysis and optimization of reaction conditions, the highest conversion of PROG was achieved at 99%, corresponding to a 14α-OH-PROG yield of 16.0 mg/L.

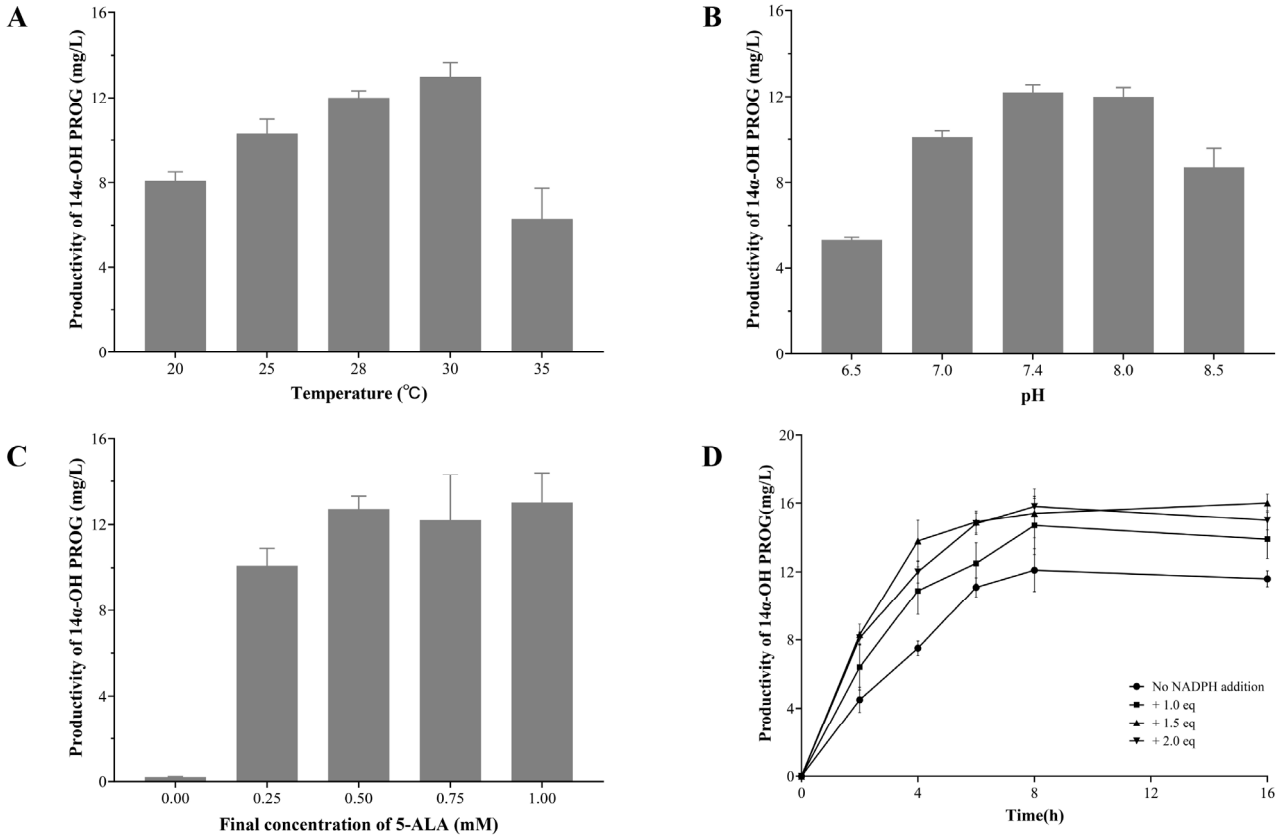


**Figure 5.** Effect of reaction conditions on the production of 14α-OH PROG in the whole-cell biocatalysis. (**A**,**B**) The effects of reaction temperature and pH on the 14α-OH PROG production. (**C**) The effects of different final concentration of 5-ALA during the expression of *P*-450$_{lun}$ on the 14α-OH PROG production. (**D**) Time course of the biotransformation with different NADPH additions. Reaction conditions: 50 g cww/L recombinant *E. coli* cells were suspended in phosphate buffer (pH 7.4, 50 mM) containing 50 μM PROG; reactions were conducted at 30 °C, 250 rpm for 16 h. Error bars are standard deviation for three independent experiments.

Thereafter, the effect of substrate concentration (ranging from 25 to 200 μM) was investigated using those optimized conditions mentioned above. The yield of 14α-OH-PROG was estimated after 8 h of transformation in the Erlenmeyer flasks. Results suggested that the maximum titer of 14α-OH-PROG was found at 50 μM substrate (Figure 6). At higher substrate concentrations (>50 μM), the accumulation of 14α-OH-PROG stopped or even showed a downward trend, which may result from the limited protein expression levels, poor substrates/products transport capacity of *E. coli* or substrates/products inhibition.

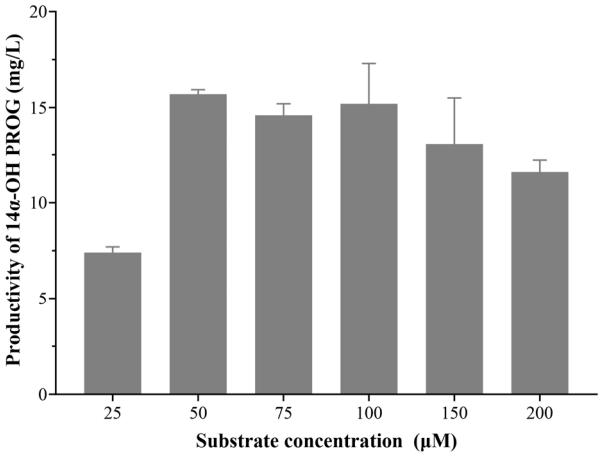


**Figure 6.** Effect of substrate concentration on the production of 14α-OH PROG in the whole-cell biocatalysis. Reaction conditions: 50 g cww/L recombinant *E. coli* cells were suspended in phosphate buffer (pH 7.4, 50 mM) containing 75 mM NADPH and varying concentration of PROG (dissolved in DMF, final 5%); reactions were conducted at 30 °C, 250 rpm for 8 h. Error bars are standard deviation for three independent experiments.

## 3. Materials and Methods

### *3.1. Strains and Reagents*

*E. coli* DH5α was used for DNA cloning and plasmid construction. *E. coli* BL21 (DE3) served as hosts for whole-cell biotransformation. Yeast extract and tryptone were purchased from Qxoid (Basingstoke, UK). Q5 Hot Start High-Fidelity DNA polymerase and restriction endonucleases were obtained from Thermo Scientific (Waltham, MA, USA). The plasmid purification kit was sourced from Omega Laboratories (Cleveland, OH, USA). Oligonucleotide synthesis and sequence analysis were performed by Novogene (Tianjin, China). PROG, 5-ALA and isopropy1 β-D-1-thiogalactopyranoside (IPTG) were purchased from Energy Chemical (Shanghai, China). Other chemicals were obtained from Genview (Beijing, China) with the highest available commercial grade.

### *3.2. Plasmid Construction and Protein Expression*

The wild-type gene *P*-$450_{lun}$ (GenBank accession numbers: MN061487) and $CPR_{lun}$ (GenBank accession numbers: MN061485) were chemically synthesized and optimized considering the codon preferences of *E. coli* by Novogene (Tianjin, China). The expression construct for the normal or modified *P*-$450_{lun}$ and $CPR_{lun}$ were designed in pRSFDuet, respectively, using primers presented in Table S1. Sequences confirmation was performed by sequencing in Novegene (Tianjin, China). The recombinant cells transformed with expression vectors (pRSFDuet) harboring the normal or modified *P*-$450_{lun}$ gene and $CPR_{lun}$ gene were cultivated at 37 °C in Luria–Bertani (LB) medium with 50 μg/mL kanamycin. In total, 0.5 mM IPTG and 0.5 mM 5-ALA were added When cells' $OD_{600}$ reached 0.6, and they continued to cultivate for 16 h at 28 °C. Then, cells were collected using centrifugation (10,000× *g*, 10 min, 4 °C) and resuspended (in 50 mM pH 7.4 potassium phosphate buffer) for the whole-cell biotransformation.

### *3.3. Whole-Cell Conversion of Progesterone Using E. coli in the Erlenmeyer flask*

In total, 10 mL potassium phosphate buffer (50 mM, pH 7.4) with 50 g cell wet weight/L (cww/L) recombinant *E. coli* and 50 μM PROG was shaken at 250 rpm and 30 °C for 8 h. In total, 2 mL samples were taken and then extracted with equal volume ethyl acetate, dried with air-blowing, re-dissolved in 200 μL chromatography methanol, and filtered through a 0.2 μm filter. Product formation was analyzed using reverse-phase HPLC to calculate the final conversions. The reaction mixture was separated by a Thermo Hypersil Gold C18 Column (4.6 × 250 mm, 5 μm) using solvent A (dd$H_2O$ with 0.1% *v*/*v*

formic acid) and solvent B (acetonitrile). The flow rate was 1 mL/min. The gradient was set as 0–15 min 30% B—95% B, 15–20 min 95% B, 20–21 min 95% B—30% B, 25 min 30% B.

### *3.4. Engineering of P-450$_{lun}$ for Improved Regioselectivity and Activity*

Single-site mutation was introduced in *P*-450$_{lun}$ with PCR using designed primers (Table S1) and Q5 hot-start high-fidelity DNA polymerase. The PCR reaction mixture (25 µL) was prepared, which included primers (1.25 µL, 10 µM), template plasmid (1 µL, 50 ng/µL), Q5 hot-start high-fidelity DNA polymerase (12.5 µL), and dd $H_2O$ (9 µL). The PCR product was digested by restriction enzyme NheI/BspTI for 1.5 h at 37 °C and then connected into corresponding restriction sites of pRSFDuet_ΔCPR$_{lun}$ using T4 DNA ligase (Thermo Scientific, Waltham, MA, USA). The final ligated products were transformed into *E. coli* BL21 (DE3) via electroporation and plated on LB agar plates containing 50 µg/mL kanamycin. Mutant colonies were inoculated in separate wells of 24-deep-well plates (0.2 mL, LB medium with 50 µg/mL kanamycin per well) and incubated at 300 rpm and 37 °C for 8 h. Then, 1.0 mL TB medium containing 50 µg/mL kanamycin, 0.5 mM IPTG, and 0.5 M 5-ALA was added to each well, and the plates continued to be incubated at 300 rpm and 28 °C for another 16 h. The cells were harvested by centrifuging the plates at 4000× *g* for 20 min, washed with 0.2 mL potassium phosphate buffer (50 mM, pH 7.4), and centrifuged again. Cells in each well were then resuspended in 0.5 mL of 50 mM pH 7.4 potassium phosphate buffer containing 50 µM PROG. The plates were shaken at 300 rpm and 30 °C for 12 h. Each sample was extracted with 500 µL ethyl acetate, dried with air-blowing, re-dissolved in 100 µL chromatography methanol, and product formation was analyzed using reverse-phase HPLC (described above). Desired mutations were confirmed using DNA sequencing.

### *3.5. Structural Modeling Analysis, Molecular Docking and Tunnel Analysis*

Swiss-Model server (https://swissmodel.expasy.org/, accessed on 10 February 2023) was used to build a 3D structure model of Δ*P*-450$_{lun}$ and its variants. To enhance the geometry and energy of the overall predicted model, energy minimization was conducted using the steepest gradient minimization algorithm, employing specific GROMACS routines. This involved performing 1500 minimization steps in a vacuum environment, with a maximum force convergence threshold set at 1.0 kJ/mol/nm. Additionally, a cut-off range of 1.4 nm was applied for both van der Waals and Coulomb interactions. Then, the optimized protein structure was refined using the GalaxyWeb server (https://galaxy.seoklab.org/index.html, accessed on 11 February 2023). The quality of the final generated model was assessed using a Ramachandran plot (SAVES server, https://saves.mbi.ucla.edu/, accessed on 12 February 2023) and Z-score (ProSA web, https://prosa.services.came.sbg.ac.at/prosa.php, accessed on 12 February 2023). Structural images were produced using PyMOL and Discovery studio visualizer 2019.

The molecular structure of the ligand PROG was constructed and optimized using ChemDraw. A grid box with dimensions of 5 Å surrounding the active site was generated, centered on the heme iron of *P*-450$_{lun}$ or its variants. Molecular docking simulations were conducted using Autodock 4.2 and subsequently visualized using PyMOL. Each variant underwent 20 docking runs, and the resulting poses were clustered based on a Root Mean Square Deviation (RMSD) cutoff of 5 Å, employing default parameters.

Tunnel analysis was performed using Caver Analyst 2.0 (https://www.caver.cz/index.php?sid=121, accessed on 17 May 2023), with the following parameters: a probe radius of 1.4 Å, shell depth of 4 Å, shell radius of 3 Å, clustering threshold of 3.5, and the starting point set at the Fe atom of the heme co-factor. Following the tunnel calculations, the bottleneck radius and tunnel-lining residues for each tunnel were extracted from the tunnel statistics and residue graph functions.

### *3.6. Optimization of the Whole-Cell Biocatalytic Process*

Optimization of bio-transformations was carried out with varying different parameters of the reactions (pH, temperature, and the additives). The whole-cell conversion process of PROG using *E. coli* containing pRSFDuet_Δ*P*-450$_{lun}$E109A/F297W_ΔCPR$_{lun}$ in the Erlenmeyer flask is similar to that mentioned above. The pH or reaction temperature varied according to different optimization purposes. Additives heme, 5-ALA or $FeSO_4 \cdot 7H_2O$ were added along with IPTG at the start of protein induction. Additive NADPH was added at the beginning of whole-cell conversion. Product formation was analyzed using reverse-phase HPLC to calculate the final yield. After all parameters were determined, the cell was induced with 0.5 M IPTG along with 0.5 mM 5-ALA. The final biocatalytic reaction was performed in 10 mL 50 mM pH 7.4 potassium phosphate buffer containing 50 g cww/L recombinant *E. coli*, 50 μM PROG and 75 μM NADPH at 30 °C for 16 h.

## 4. Conclusions

This study described the successful expression and development of the *C. lunatus* derived steroid 14α-hydroxylase *P*-450$_{lun}$ in the *E. coli* expression system. The N-terminal hydrophobic region truncated strategy was applied to express the eukaryotic membrane protein *P*-450$_{lun}$ and its cognate partner CPR$_{lun}$ in *E. coli*. Using a semi-rational design and directed evolution, a Δ*P*-450$_{lun}$ variant E109A/F297W with ~97% regioselectivity to the C14α position of PROG was obtained. Then, whole-cell catalyzed reaction conditions were optimized, and the final yield of 14α-OH-PROG was approximately 16.0 mg/L. The *E. coli* system obtained in this study can serve as a basis to produce 14α-OH-PROG and a rapid evolution platform to eukaryotic cytochrome *P*-450$_{lun}$. Nonetheless, the yield and productivity of this system are still low. Thus, research is underway to construct a NADPH regeneration system in host cells, promote the transportation of hydrophobic substrates and products, and further increase the catalytic activity of *P*-450$_{lun}$.

**Supplementary Materials:** The following supporting information can be downloaded at https://www.mdpi.com/article/10.3390/catal14040247/s1. Table S1: List of primers using in this article; Figure S1: ProSA Z-Score result of the Δ*P*-450$_{lun}$ model. Figure S2: Ramachandran Plot of the structure of Δ*P*-450$_{lun}$. Figure S3: $^{1}$H-NMR spectrum of isolated 11β-OH PROG (600 MHz, $CDCl_3$). Figure S4: $^{13}$C-NMR spectrum of isolated 11β-OH PROG (600 MHz, $CDCl_3$). Figure S5: $^{1}$H-NMR spectrum of isolated 14α-OH PROG (600 MHz, $CDCl_3$). Figure S6: $^{13}$C-NMR spectrum of isolated 14α-OH PROG (600 MHz, $CDCl_3$). Figure S7: Binding pocket properties of Δ*P*-450$_{lun}$ and Δ*P*-450$_{lun}$-F297W.

**Author Contributions:** Y.C.: conceptualization, methodology, visualization, writing—original draft preparation. H.L.: investigation validation, data curation. W.T.: validation, software. Z.C.: project administration, supervision, writing—review and editing. All authors have read and agreed to the published version of the manuscript.

**Funding:** This research received no external funding.

**Data Availability Statement:** The original contributions presented in the study are included in the article/Supplementary Materials; further inquiries can be directed to the corresponding author/s.

**Acknowledgments:** I would like to thank the anonymous reviewers who have helped to improve the paper.

**Conflicts of Interest:** Author Zunxue Chang was employed by the company Shenyang Botai Biopharmaceutical Co., Ltd. The remaining authors declare that the research was conducted in the absence of any commercial or financial relationships that could be construed as a potential conflict of interest.

## References


1. Cutolo, M.; Straub, R.H. Sex steroids and autoimmune rheumatic diseases: State of the art. *Nat. Rev. Rheumatol.* **2020**, *16*, 628–644. [CrossRef]
2. Zhang, M.; Bai, X.; Cao, W.; Ji, J.; Wang, L.; Yang, Y.; Yang, H. The influence of corticosteroids, immunosuppressants and biologics on patients with inflammatory bowel diseases, psoriasis and rheumatic diseases in the era of COVID-19: A review of current evidence. *Front. Immunol.* **2021**, *12*, 677957. [CrossRef] [PubMed]
3. Chasalow, F. An Introduction to Spiral Steroids. *Int. J. Mol. Sci.* **2022**, *23*, 9523. [CrossRef]
4. Ogino, Y.; Sato, T.; Lguchi, T. *Gonadal Steroids*; Academic Press: New York, NY, USA, 2021.
5. Chen, W.; Fisher, M.J.; Leung, A.; Cao, Y.; Wong, L.L. Oxidative diversification of steroids by nature-inspired scanning glycine mutagenesis of P450BM3 (CYP102A1). *ACS Cat.* **2020**, *10*, 8334–8343. [CrossRef]
6. Andryushina, V.A.; Voishvillo, N.E.; Druzhinina, A.V.; Stytsenko, T.S.; Yaderets, V.V.; Petrosyan, M.A.; Zeinalov, O.A. 14α-Hydroxylation of steroids by mycelium of the mold fungus *Curvularia lunata* (VKPM F-981) to produce precursors for synthesizing new steroidal drugs. *Pharm. Chem. J.* **2013**, *47*, 102–108. [CrossRef]
7. Hu, S.H.; Genain, G.; Azerad, R. Microbial transformation of steroids: Contribution to 14α-hydroxylations. *Steroids* **1995**, *60*, 337–352. [CrossRef] [PubMed]
8. Takara, Y.; Masaaki, F.; Yasuko, F.; Jo, K.; Masamichi, N.; Makoto, Y.; Hiroji, O. Inhibitory effect of a new androstenedione derivative, 14α-hydroxy-4-androstene-3, 6, 17-trione (14α-OHAT) on aromatase activity of human uterine tumors. *J. Steroid Biochem.* **1990**, *36*, 517–521. [CrossRef] [PubMed]
9. Rieck, C.; Geiger, D.; Munkert, J.; Messerschmidt, K.; Petersen, J.; Strasser, J.; Meitinger, N.; Kreis, W. Biosynthetic approach to combine the first steps of cardenolide formation in *Saccharomyces cerevisiae*. *MicrobiologyOpen* **2019**, *8*, e925. [CrossRef]
10. Sales, E.; Müller-Uri, F.; Nebauer, S.G.; Segura, J.; Kreis, W.; Arrillaga, I. Digitalis. In *Wild Crop Relatives: Genomic and Breeding Resources: Plantation and Ornamental Crops*; Springer: Berlin/Heidelberg, Germany, 2011; pp. 73–112. [CrossRef]
11. Züst, T.; Mirzaei, M.; Jander, G. Erysimum cheiranthoides, an ecological research system with potential as a genetic and genomic model for studying cardiac glycoside biosynthesis. *Phytochem. Rev.* **2018**, *17*, 1239–1251. [CrossRef]
12. Wife, R.L.; Kyle, D.; Mulheirn, L.J.; Volger, H.C. Selective hydrocarbon oxidation: Dry ozonation of steroids on silica. *J. Chem. Soc. Chem. Commun.* **1982**, *5*, 306–307. [CrossRef]
13. Athelstan, L.J.B.; Thach, D. Regioselective oxidation of unactivated methylene and methine groups by dry ozonation: Similarity to microbiological oxidation. *J. Chem. Soc. Chem. Comm.* **1978**, *9*, 2473–2670. [CrossRef]
14. Ciaramella, A.; Minerdi, D.; Gilardi, G. Catalytically self-sufficient cytochromes P450 for green production of fine chemicals. *Rend. Fis. Acc. Lincei* **2016**, *28*, 169–181. [CrossRef]
15. Chen, J.; Tang, J.L.; Xi, Y.Y.; Dai, Z.B.; Bi, C.H.; Chen, X.; Fan, F.Y.; Zhang, X.L. Production of 14α-hydroxysteroids by a recombinant *Saccharomyces cerevisiae* biocatalyst expressing of a fungal steroid 14α-hydroxylation system. *Appl. Microbiol. Biotechnol.* **2019**, *103*, 8363–8374. [CrossRef]
16. Kristan, K.; Rizner, T.L. Steroid-transforming enzymes in fungi. *J. Steroid Biochem.* **2012**, *129*, 79–91. [CrossRef]
17. Zhao, Y.; Zhang, B.; Sun, Z.Q.; Zhang, H.; Wang, W.; Wang, Z.R.; Guo, Z.K.; Yu, S.; Tan, R.X.; Ge, H.M. Biocatalytic C14-Hydroxylation on androstenedione enabled modular synthesis of cardiotonic steroids. *ACS Cat.* **2022**, *12*, 9839–9845. [CrossRef]
18. Song, F.Z.; Zheng, M.M.; Wang, J.L.; Liu, H.H.; Lin, Z.; Liu, B.B.; Deng, Z.X.; Cong, H.J.; Zhou, Q.H.; Qu, X.D. Chemoenzymatic synthesis of C14-functionalized steroids. *Nat. Synth.* **2023**, *2*, 729–739. [CrossRef]
19. Felpeto-Santero, C.; Galan, B.; Luengo, J.M.; Fernandez-Canon, J.M.; Del Cerro, C.; Medrano, F.J.; Garcia, J.L. Identification and expression of the 11beta-steroid hydroxylase from *Cochliobolus lunatus* in *Corynebacterium glutamicum*. *Microb. Biotechnol.* **2019**, *12*, 856–868. [CrossRef]
20. Zhang, C.; Shen, Y.; Gao, Y.; Zan, Z.; Wang, M. Efficient production of 14α-OH-AD by engineered Mycolicibacterium neoaurum via coupled cofactor and reconstructed electron transport system. *Syst. Microbiol. Biomanuf.* **2023**, *3*, 358–369. [CrossRef]
21. Permana, D.; Niesel, K.; Ford, M.J.; Ichinose, H. Latent functions and applications of cytochrome P450 monooxygenases from *Thamnidium elegans*: A novel biocatalyst for 14alpha-hydroxylation of Testosterone. *ACS Omega* **2022**, *7*, 13932–13941. [CrossRef]
22. Pessôa, M.T.C.; Barbosa, L.A.; Villar, J.A.F. Synthesis of cardiac steroids and their role on heart failure and cancer. *Stud. Nat. Prod. Chem.* **2018**, *57*, 79–113. [CrossRef]
23. Boer, E.; Steinborn, G.; Kunze, G.; Gellissen, G. Yeast expression platforms. *Appl. Microbiol. Biotechnol.* **2007**, *77*, 513–523. [CrossRef] [PubMed]
24. Alder, N.N.; Johnson, A.E. Cotranslational membrane protein biogenesis at the endoplasmic reticulum. *J. Biol. Chem.* **2004**, *279*, 22787–22790. [CrossRef] [PubMed]
25. Freigassner, M.; Pichler, H.; Glieder, A. Tuning microbial hosts for membrane protein production. *Microb. Cell Fact.* **2009**, *8*, 69. [CrossRef] [PubMed]
26. Gordon, E.; Horsefield, R.; Swarts, H.G.; de Pont, J.J.; Neutze, R.; Snijder, A. Effective high-throughput overproduction of membrane proteins in *Escherichia coli*. *Protein Expr. Purif.* **2008**, *62*, 1–8. [CrossRef] [PubMed]
27. Shumyantseva, V.V.; Bulko, T.; Shich, E.; Makhova, A.; Kuzikov, A.; Archakov, A. Cytochrome P450 enzymes and electrochemistry: Crosstalk with electrodes as redox partners and electron sources. *Adv. Exp. Med. Biol.* **2015**, *851*, 229–246. [CrossRef]
28. Li, S.; Du, L.; Bernhardt, R. Redox partners: Function modulators of bacterial P450 enzymes. *Trends Microbiol.* **2020**, *28*, 445–454. [CrossRef] [PubMed]

29. Kerrigan, J.J.; Xie, Q.; Ames, R.S.; Lu, Q. Production of protein complexes via co-expression. *Protein Expr. Purif.* **2011**, *75*, 1–14. [CrossRef]
30. Mizuguchi, H.; Xu, Z.; Ishii-Watabe, A.; Uchida, E.; Hayakawa, T. IRES-dependent second gene expression is significantly lower than cap-dependent first gene expression in a bicistronic vector. *Mol. Ther.* **2000**, *1*, 376–382. [CrossRef] [PubMed]
31. Kim, K.J.; Kim, H.E.; Lee, K.H.; Han, W.; Yi, M.J.; Jeong, J.; Oh, B.H. Two-promoter vector is highly efficient for overproduction of protein complexes. *Protein Sci.* **2004**, *13*, 1698–1703. [CrossRef]
32. Chen, X.; Zaro, J.L.; Shen, W.C. Fusion protein linkers: Property, design and functionality. *Adv. Drug Deliv. Rev.* **2013**, *65*, 1357–1369. [CrossRef]
33. Yu, K.; Liu, C.; Kim, B.G.; Lee, D.Y. Synthetic fusion protein design and applications. *Biotechnol. Adv.* **2015**, *33*, 155–164. [CrossRef] [PubMed]
34. van Rosmalen, M.; Krom, M.; Merkx, M. Tuning the flexibility of Glycine-Serine linkers to allow rational design of multidomain proteins. *Biochemistry* **2017**, *56*, 6565–6574. [CrossRef] [PubMed]
35. Snijder, H.J.; Hakulinen, J. Membrane protein production in *E. coli* for applications in drug discovery. *Adv. Exp. Med. Biol.* **2016**, *896*, 59–77. [CrossRef] [PubMed]
36. Hu, B.; Zhao, X.; Wang, E.; Zhou, J.; Li, J.; Chen, J.; Du, G. Efficient heterologous expression of cytochrome P450 enzymes in microorganisms for the biosynthesis of natural products. *Crit. Rev. Biotechnol.* **2023**, *43*, 227–241. [CrossRef] [PubMed]
37. Cosme, J.; Johnson, E.F. Engineering Microsomal Cytochrome P450 2C5 to Be a Soluble, Monomeric Enzyme: Mutations That Alter Aggregation, Phospholipid Dependence of Catalysis, and Membrane Binding. *J. Biol. Chem.* **2000**, *275*, 2545–2553. [CrossRef] [PubMed]
38. Tang, Z.; Salamanca-Pinzon, S.G.; Wu, Z.L.; Xiao, Y.; Guengerich, F.P. Human cytochrome P450 4F11: Heterologous expression in bacteria, purification, and characterization of catalytic function. *Arch. Biochem. Biophys.* **2010**, *494*, 86–93. [CrossRef] [PubMed]
39. Chen, X.; Zhang, C.; Too, H.P. Multienzyme biosynthesis of dihydroartemisinic acid. *Molecules* **2017**, *22*, 1422. [CrossRef] [PubMed]
40. Zelasko, S.; Palaria, A.; Das, A. Optimizations to achieve high-level expression of cytochrome P450 proteins using *Escherichia coli* expression systems. *Protein Expr. Purif.* **2013**, *92*, 77–87. [CrossRef]
41. Waterhouse, A.; Bertoni, M.; Bienert, S.; Studer, G.; Tauriello, G.; Gumienny, R.; Heer, F.T.; de Beer, T.A.P.; Rempfer, C.; Bordoli, L.; et al. SWISS-MODEL: Homology modelling of protein structures and complexes. *Nucleic Acids Res.* **2018**, *46*, W296–W303. [CrossRef]
42. Sevrioukova, I.F. High-Level Production and Properties of the Cysteine-Depleted Cytochrome P450 3A4. *Biochemistry* **2017**, *56*, 3058–3067. [CrossRef]
43. Gricman, L.; Vogel, C.; Pleiss, J. Conservation analysis of class-specific positions in cytochrome P450 monooxygenases: Functional and structural relevance. *Proteins* **2014**, *82*, 491–504. [CrossRef] [PubMed]
44. Shin, W.H.; Lee, G.R.; Heo, L.; Lee, H.; Seok, C.J.B.D. Prediction of protein structure and interaction by GALAXY protein modeling programs. *BioDesign* **2014**, *2*, 1–11.
45. Seok, C.; Baek, M.; Steinegger, M.; Park, H.; Lee, G.R.; Won, J. Accurate protein structure prediction: What comes next? *BioDesign* **2021**, *9*, 47–50. [CrossRef]
46. Pronk, S.; Pall, S.; Schulz, R.; Larsson, P.; Bjelkmar, P.; Apostolov, R.; Shirts, M.R.; Smith, J.C.; Kasson, P.M.; van der Spoel, D.; et al. GROMACS 4.5: A high-throughput and highly parallel open source molecular simulation toolkit. *Bioinformatics* **2013**, *29*, 845–854. [CrossRef] [PubMed]
47. Wiederstein, M.; Sippl, M.J. ProSA-web: Interactive web service for the recognition of errors in three-dimensional structures of proteins. *Nucleic Acids Res.* **2007**, *35*, W407–W410. [CrossRef] [PubMed]
48. Lüthy, R.; Bowie, J.U.; Eisenberg, D. Assessment of protein models with three-dimensional profiles. *Nature* **1992**, *356*, 83–85. [CrossRef] [PubMed]
49. Bowie, J.U.; Lüthy, R.; Eisenberg, D. A method to identify protein sequences that fold into a known three-dimensional structure. *Science* **1991**, *253*, 164–170. [CrossRef] [PubMed]
50. Seifert, A.; Pleiss, J. Identification of selectivity-determining residues in cytochrome P450 monooxygenases: A systematic analysis of the substrate recognition site 5. *Proteins* **2009**, *74*, 1028–1035. [CrossRef] [PubMed]
51. Khatri, Y.; Jozwik, I.K.; Ringle, M.; Ionescu, I.A.; Litzenburger, M.; Hutter, M.C.; Thunnissen, A.W.H.; Bernhardt, R. Structure-Based engineering of steroidogenic CYP260A1 for stereo- and regioselective hydroxylation of progesterone. *ACS Chem. Biol.* **2018**, *13*, 1021–1028. [CrossRef]
52. Kokkonen, P.; Bednar, D.; Pinto, G.; Prokop, Z.; Damborsky, J. Engineering enzyme access tunnels. *Biotechnol. Adv.* **2019**, *37*, 107386. [CrossRef]
53. Banerjee, R.; Lipscomb, J.D. Small-molecule tunnels in metalloenzymes viewed as extensions of the active site. *Acc. Chem. Res.* **2021**, *54*, 2185–2195. [CrossRef] [PubMed]
54. Chovancova, E.; Pavelka, A.; Benes, P.; Strnad, O.; Brezovsky, J.; Kozlikova, B.; Damborsky, J. CAVER 3.0: A tool for the analysis of transport pathways in dynamic protein structures. *PLoS Comput. Biol.* **2012**, *8*, e1002708. [CrossRef] [PubMed]
55. Cojocaru, V.; Winn, P.J.; Wade, R.C. The ins and outs of cytochrome P450s. *Biochim. Biophys. Acta (BBA)-Gen. Subj.* **2007**, *1770*, 390–401. [CrossRef] [PubMed]

56. Cheng, Z.Y.; Cui, W.J.; Liu, Z.M.; Zhou, L.; Wang, M.; Kobayashi, M.; Zhou, Z.M. A switch in a substrate tunnel for directing regioselectivity of nitrile hydratases towards α, ω-dinitriles. *Catal. Sci. Technol.* **2016**, *6*, 1292–1296. [CrossRef]
57. Meng, S.Q.; An, R.P.; Li, Z.Y.; Schwaneberg, U.; Ji, Y.; Davari, M.D.; Wang, F.; Wang, M.; Qin, M.; Nie, K.; et al. Tunnel engineering for modulating the substrate preference in cytochrome $P450_{Bs\beta}$ HI. *Bioresour. Bioprocess.* **2021**, *8*, 26. [CrossRef]
58. Feng, C.; Pan, M.; Tang, L. 5-Aminolevulinic acid level and dye-decolorizing peroxidase expression regulate heme synthesis in *Escherichia coli*. *Biotechnol. Lett.* **2022**, *44*, 271–277. [CrossRef]
59. Quehl, P.; Hollender, J.; Schüürmann, J.; Brossette, T.; Maas, R.; Jose, J. Co-expression of active human cytochrome P450 1A2 and cytochrome P450 reductase on the cell surface of *Escherichia coli*. *Microb. Cell Fact.* **2016**, *15*, 26. [CrossRef]